DOI:
10.1021/acscatal.6b00259

Document Version
Publisher's PDF, also known as Version of record

ACS Catalysis

Research Article

pubs.acs.org/acscatalysis

"Get in Touch and Keep in Contact": Interface Effect on the Oxygen Reduction Reaction (ORR) Activity for Supported PtNi Nanoparticles

Gian Giacomo Asara,*[,†] Lauro Oliver Paz-Borbón,[†,‡] and Francesca Baletto*[,†]

[†]Physics Department, King's College London, Strand WC2R 2LS, United Kingdom

[‡]Instituto de Fisica, Universidad Nacional Autónoma de México, Apdo. Postal 20-364, 01000 Mexico, D.F. Mexico

Supporting Information

ABSTRACT: Elucidating the interplay between shape, chemical composition, and catalytic activity is an essential task in the rational nanocatalyst design process. We investigated the activity of MgO-supported PtNi nanoalloys of ∼1.5 nm toward the oxygen reduction reaction using first-principles simulations. Cuboctahedral-shaped particles result to be more active than truncated octahedra of similar sizes, and alloying produces a quantitative improvement in the catalytic activity independent of the catalyst morphology. Our results suggest a practical recipe for catalyst nanoengineering controlling the chemical composition at the metal/oxide interface. Indeed, Ni atoms in contact with the oxide support reduce the binding energy of molecular oxygen at different adsorption sites.

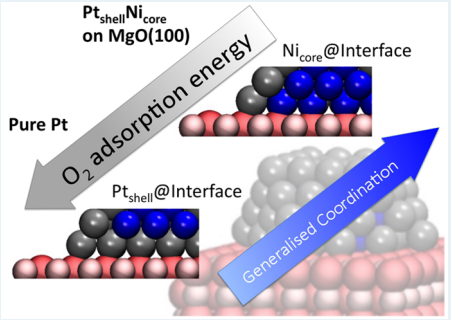

KEYWORDS: *ORR, Pt, nanoparticle, nanoalloy, core−shell, generalized coordination number, PEMFC, catalyst-by-design*

INTRODUCTION

Nanocatalysis is a rapidly growing technology widely applied in chemical synthesis and energy storage. Heterogeneous nanocatalysts are composed by metallic nanoparticles (NPs) ranging from aggregates of tens of atoms to nanoarchitectures of several thousands, dispersed or encapsulated onto supports.[1] The control of particle size, morphology, and chemical composition, while ensuring thermal and chemical stability, allows the production of selective long-lifetime nanocatalysts that present high activity, compared to bulk materials. Understanding the molecular mechanisms behind the high catalytic activity of metallic nanoalloys, together with the prediction of their structural stability, are key steps in engineering alternative materials with same or improved catalytic performance but presenting lower manufacturing costs and higher poisoning resistance.[2−4]

Pt nanoparticles are widely employed as nanocatalysts. For example, they are the active constituent of electrodes used in proton exchange membrane fuel cells (PEMFCs). However, they exhibit sluggish kinetics for the reduction of molecular oxygen (oxygen reduction reaction, ORR), the semireaction at the cathode, which is one of the main hindrances for their application in the automotive industry.[5,6] The ORR rate can be improved via deposition of a thin Pt shell over a transition-metal core[7] of Au,[8] Cu,[9] and Ni,[10−13] in place of the pure Pt electrode. Moreover, alloyed and doped Pt nanoclusters display a better resistance to poisoning.[14,15] It was recently shown that platonic shapes,[16] but also dealloyed[17] nanoporous structures, yield to very active PtNi nanocatalysts for ORR reaction. One of the open questions is then related to the description of a "catalyst-by-design" route instead of a "mixing and baking" or "trial and error" procedure.

The structural characterization of a metallic nanoparticle and the mapping of its active sites, the so-called "chemisorption" map, provides a path to rationalize and manipulate the physicochemical properties of a cluster. Numerical modeling based on density functional theory (DFT) is a very robust aid in nanocatalyst design, which allows one to discern and disentangle the effect of shape, chemical composition, and interaction with the support.[18]

This work focuses on the molecular oxygen adsorption, the starting point of any mechanisms for the ORR, and it aims to clarify how the morphology and the chemical ordering of supported PtNi clusters affects the chemisorption of O_2 at different sites. According to the Sabatier principle[19] and following the observation that the rate-limiting steps for the ORR upon Pt_3Ni and PtNi surfaces are the dissociation and/or protonation of molecular oxygen,[20,21] a rational design of these nanoalloys will seek to weaken the O_2 interaction with the metallic NP. Free and small PtNi nanoalloys, up to ∼50 atoms, bind O_2 too strongly and therefore undergo significant adsorbate-induced distortions, resulting in an inability to catalyze ORR.[22] MgO-supported nanoparticles at sizes smaller than 58 atoms still show severe rearrangements, making the alloying effect not so clear.[23] Here, we considered a cuboctahedron (CO) of 86 atoms and a truncated octahedron (TO) of 82 atoms, with an approximate diameter of 1.5 nm, both soft-landed on MgO(100). For those larger sizes, we did not observe any severe rearrangements, even after the adsorption of O_2. The adsorption map of the supported

Received: January 26, 2016
Revised: May 17, 2016
Published: May 31, 2016

DOI: 10.1021/acscatal.6b00259
ACS Catal. 2016, 6, 4388−4393

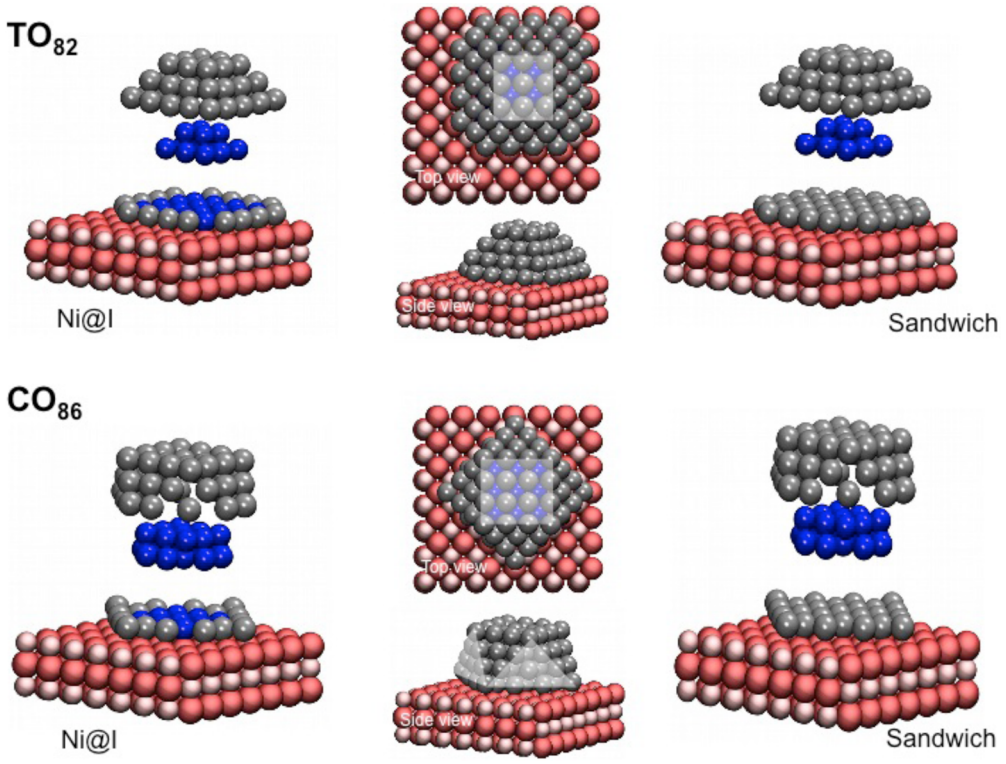

Figure 1. TO_{82} and CO_{86} are shown in the top and bottom rows, respectively. The central column reports the top and side view of the clusters, where (100) facets are shadowed. A pictorial decomposition along the direction perpendicular to the substrate is sketched on the left and right panels for the Ni@I and sandwich chemical orderings, respectively. Pt atoms are shown in gray, Ni are shown in blue, and red and pink represent O and Mg atoms, respectively.

bimetallic nanoparticles is proposed and discussed in terms of the generalized coordination number (GCN). The GCN, recently introduced by Sautet and co-workers, is a new descriptor as robust as the center of the *d*-band, which establishes a direct link between geometry and adsorption map as well as activity.[24−26] At the best of our knowledge, this is the first study where the GCN is calculated and used for oxide-supported bimetallic systems.

Interestingly, we found that the chemical composition at the oxide interface tunes the chemisorption map and then likely the catalytic activity. A few Ni atoms in contact with the MgO substrate turn a PtNi cuboctahedron into a very promising nanocatalyst for ORR.

COMPUTATIONAL METHOD

We perform periodic density functional theory (DFT) calculations using a slab model approach. All calculations are performed using the VASP package.[27] We consider two different geometries: a cuboctahedron (CO) and a truncated octahedron (TO) of 86 and 82 atoms, respectively (see Figure 1). They are both obtained from larger CO and TO of 147 and 201 atoms, cut and deposited along the {100} plane. We considered $Pt_{shell}Ni_{core}$ systems give Pt a tendency to segregate to the uppermost shell, because of its larger dimensions and lower surface energy.[20] According to recent computer simulations and experiments, the lack of vacancies in the Ni_{core} reduces the Ni dissolution rate substantially, stabilizing $Pt_{shell}Ni_{core}$ chemical ordering.[28−30] Since very small Ni clusters have a tendency to flatten and oxidize,[31] it is likely that Ni atoms try to segregate at the interface instead of at the cluster surface. Therefore, two chemical arrangements are examined: the "sandwich" configuration, a proper $Pt_{shell}Ni_{core}$ ordering with a pure Pt monolayer in contact with the substrate and the "Ni at the interface (Ni@I)", where mainly Ni atoms are touching the oxide. We considered a $Pt_{65}Ni_{21}$ (sandwich) and a $Pt_{56}Ni_{30}$ (Ni@I) with CO_{86} morphology, corresponding to 75.6% Pt and 65% Pt, respectively; a $Pt_{69}Ni_{13}$ (sandwich) and a $Pt_{53}Ni_{29}$ (Ni@I) for the TO_{82} shape, where the Pt loading is at 84% and 65%, respectively. A schematic representation of our systems and their chemical ordering is provided in Figure 1.

Each nanoarchitecture was deposited onto a MgO (7 × 7) supercell composed by three atomic layers frozen in their optimized bulk atomic position (a = 4.238 Å). Interaction between replicas along the z-axis is avoided, separating them by ∼17 Å, while clusters are at least ∼5 Å far apart in the xy-plane.

Although magnesium oxide may be not the best material for an electrode, it provides a very good platform to tackle the epitaxial strain effects induced into the metallic systems. Among other oxide substrates, it acts as a paradigmatic example of an almost rigid, strongly interacting support. It has a single, well-characterized, nonreducible crystal phase showing a stable nonpolar (001) surface. MgO is widely used in experiments,[32] and from the computational point of view, it can be accurately treated with standard *ab initio* methods, because it does not have any peculiar magnetic behavior. Within the standard DFT framework, the exchange and correlation contribution to the total energy of the system has been estimated using the PBE flavor of the generalized gradient approximation.[33] The valence electrons of the system are represented using a plane wave (PW) basis set whose associated maximum kinetic energy did not exceed the value of 380 eV, whereas the core electrons have been described according to the projected augmented wave

DOI: 10.1021/acscatal.6b00259
ACS Catal. 2016, 6, 4388−4393

(PAW) approximation.[34] Thus, 2 valence electrons have been considered explicitly for each Mg atom, 6 for each O atom, and 10 for each Ni or Pt atom. Sampling in the reciprocal space has been performed at the Γ-point. The self-consistent procedure for the optimization of the wave function was performed until the energies calculated in two subsequent steps differed by <1 meV.

Spin polarization was included to properly describe the open-shell nature of the oxygen molecule and the magnetic behavior of Ni and Pt at the nanoscale.[35,36] Dipole correction was applied perpendicularly to the oxide surface. Deposited nanoparticles showed a finite magnetic moment in the range of 26−37 Bohr magnetons. In Table SI 1 in the Supporting Information, we compare the total magnetization of pure Pt, pure Ni, and PtNi NPs in the gas phase and oxide-supported. During each geometrical optimization, the metallic cluster and the molecule were relaxed using a conjugate-gradient algorithm until forces on atoms were <0.05 eV/Å. This computational setup proved to be accurate enough for a description of the basic physics of the system and for the purpose of this work. Test calculations using stricter convergence criteria (maximum kinetic energy of <415 eV, forces of <0.03 eV/Å) produce tiny variations in the calculated adsorption energies and geometries, while retaining the relative energy order among adsorption sites.

We would like to briefly comment on the stability of the $Pt_{shell}Ni_{core}$ systems. A rather detailed investigation of the mechanism and kinetic of degradation is presented in ref 17. However, it has been observed that the core−shell chemical ordering has a sufficiently long lifetime to be detected experimentally,[37] and, generally speaking, chemical reordering can be a complex and slow process.[38] In the eventuality that Ni atoms migrate from the core to the uppermost layer, one can expect a stronger binding of the oxygen molecule, as it has been shown in the gas phase.[22] The stability of supported PtNi nanoalloys can be also discussed in terms of their adhesion energy (E_{adh}), defined as the energy difference between the relaxed structure after/before the deposition. As reported in Table SI 2 in the Supporting Information, E_{adh} has a tendency to increase when Ni atoms are present at the interface. TO_{82} and CO_{86} have 32 and 25 interfacial atoms, respectively, with a E_{adh} value *per contact atom* of ∼0.4−0.6 eV. Note that the considered shapes have different wetting angles, calculated as the dihedral angle between the vector normal to the surface of the nanoparticle and the vector lying on the MgO(001) surface. For (111) facets, the wetting angle varies between 126.8° to 135°, following the order CO (sandwich) < TO (sandwich) ≤ TO (Ni@I) ≪ CO (Ni@I).

The extent of the interaction between the oxygen molecule and the nanoparticle, hereafter referred as adsorption or chemisorption energy (E_{ads}), is calculated as

$$E_{ads} = -(E_{supN+O_2} - E_{supN} - E_{O_2}) \quad (1)$$

where E_{supN+O_2} is the total energy of the supported nanocluster and adsorbed O_2 molecule system and E_{supN} and E_{O_2} are the energies of the clean supported metallic nanoparticle and of the relaxed O_2 molecule, respectively. According to this definition, a stronger interaction is associated with a more positive value of E_{ads}. Adsorption involving Pt atoms of the inferior layer of the NP in direct contact with the oxide was intentionally disregarded.

In order to differentiate the chemical environment of each adsorption site, despite the shape, composition, and size of the cluster, we calculate the generalized coordination number (GCN) per each site.[24,25] The GCN of a site i is defined as its coordination number weighted by the coordination of its neighboring atoms:

$$GCN(i) = \sum_{j=1}^{n_i} \frac{CN(j)}{CN_{max}} \quad (2)$$

where the sum runs over all nearest neighbors n_i of each atom i of a given site. Each neighbor counts then as its coordination number divided by the maximum coordination number of that adsorption site. The threshold distance to calculate the coordination number is based on the pair distribution function (see Figure SI 1 in the Supporting Information). It is important to note that, besides the mismatch between Pt and Ni, it is possible to clearly identify the peak of the first neighbor shell. We found that it is not necessary to explicitly differentiate the two chemical species, as discussed in the Supporting Information. Indeed, the effect of a different weight per each chemical species based on their Pauling electronegativity has a negligible effect on the linear fitting of the chemisorption energies against the GCN (see Figure SI 2 in the Supporting Information). Therefore, we opt to use the simplest formulation, as described in eq 2.

In our case, we keep CN_{max} = 18, because the molecular oxygen adsorption always occurs in a on-top on-top configuration, over two atoms of the Pt_{shell}. GCN can distinguish symmetrically equivalent sites, rationalizing their different chemisorption energies since weaker interaction occurs where generalized coordination is higher.[26] Hence, it is possible to define ranges for which adsorption is favored but still weak enough to improve the ORR activity, compared to pure Pt. The GCN allows to analyze the E_{ads} as a function of the coordination of the adsorption site, to directly compare nanoclusters with different compositions, and to discriminate the effect of the substrate.

RESULTS AND DISCUSSION

Despite their reduced dimensions, PtNi clusters exhibit a variety of nonequivalent adsorption sites (NEAS) intrinsic in their morphology. We count 7 and 9 NEAS for the TO_{82} and CO_{86}, respectively. We consider only on-top on-top sites, where each O atom of the molecule interacts with one Pt atom. For the sake of clarity, we group NEAS on the basis of the geometrical position of the Pt-bridge underneath O_2, as depicted in Figure 2. For example, "Vertex-Edge" means that O_2 adsorbs on a vertex and one of its nearest neighbor along an edge; similarly, $(111)^2$ and $(100)^2$ stand for a molecule upon a (111) or (100) facet, respectively.

The same nomenclature in Figure 2 is used in Figure 3, where the adsorption energies are reported and compared against pure Pt and Ni cuboctahedra and truncated octahedra. As expected, the adsorption on pure Ni is much stronger than Pt, and generally TO_{82} has a tendency to bind O_2 more than CO_{86}.

Figure 3 forecasts an improvement in the ORR activity after alloying. On ∼1.5 nm PtNi nanoalloys (red and black symbols) the adsorption energies range is 0.1−1.5 eV, which is usually weaker than on pure Pt clusters (blue symbols), and, on average, it is reduced, compared to extended Pt surfaces (green dotted lines from ref 39). Surprisingly, the contact between the

DOI: 10.1021/acscatal.6b00259
ACS Catal. 2016, 6, 4388−4393

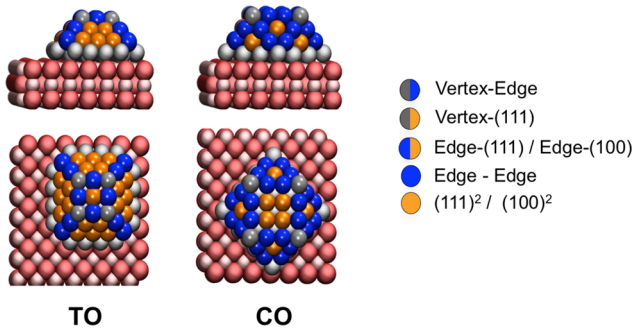

Figure 2. Nonequivalent adsorption sites nomenclature. In the left and middle panels, the color-code distinguishes geometrically equivalent atomic positions; atoms on facet are orange, atoms on the edge are blue; atoms on the vertex are gray. Each adsorption site is defined following the legend on the right panel. A full orange (blue) circle refers to the adsorption on two Pt atoms of a facet (edge); the two-color symbols indicate adsorption over two geometrical different atoms: vertex–edge (gray–blue), vertex–facet (gray–orange), and edge–facet (blue–orange).

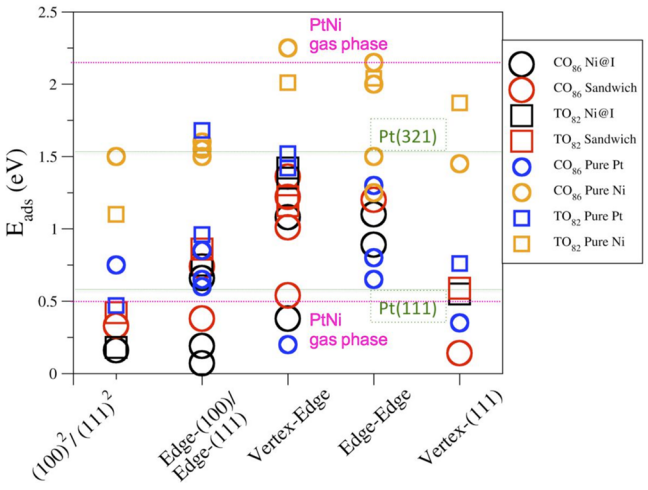

Figure 3. DFT-calculated adsorption energy (E_{ads}) (eV) for O_2 on CO_{86} (circles, ○) and TO_{82} (squares, □) for pure Pt (blue) and Ni (orange) and for PtNi Ni@I (black) and sandwich (red) clusters. Each adsorption site follows the nomenclature given in Figure 2. For reference, green dotted lines are values for adsorption on Pt(111) and stepped Pt(321), taken from ref 39; magenta lines refer to the weakest and strongest adsorption on the gas phase PtNi clusters, taken from ref 22.

Ni_{core} and the oxide reduces the O_2 adsorption energy on all sites. For example, upon a TO_{82}(111) facet, E_{ads} is reduced from 0.4 eV for "sandwich" chemical ordering to 0.2 eV for the Ni@I case. On sites where O_2 bridges an atom of the (100) facet with one of the edge, E_{ads} changes from 0.9 eV to 0.7 eV. A similar trend is observed on the CO_{86}. Furthermore, the presence of Ni atoms at the interface in the TO broadens the adsorption energy window, with respect to the sandwich chemical ordering, from 0.8 eV to 1.3 eV. We would like to note that the number of sites within an adsorption energy range can be tuned by the chemical composition of the interface layer. Referring to the upper limit for the binding energy of molecular oxygen on Pt(111),[19,40] the number of sites with $E_{ads} \leq 0.75$ eV increases from two to three on the TO_{82} and from four to five on the CO_{86} when Ni atoms touch the MgO. We would like to highlight the size and the support effects. Decreasing the NP size seems to produce an increase in E_{ads}, while the presence of the oxide support results in a general weakening of the interaction with O_2. DFT calculations on supported PtNi nanoparticles with <58 atoms show an adsorption energy window of 0.2−1.9 eV;[23] whereas, in the gas phase, the adsorption energy window of PtNi nanoalloys (magenta lines in Figure 3) is 0.5−2.2 eV.[22]

As expected, the less-coordinated sites, featuring edge or vertex atoms, show stronger binding. Notwithstanding, the relationship between the calculated adsorption energy and nominal total coordination number is far from straightforward. A quantitative analysis of the geometrical strain, induced by a different chemical composition at the interface and by the presence of the support, can be rationalized in terms of the generalized coordination number, as defined in eq 2. The GCN of same type of adsorption site may vary largely from one structure to another, depending on the alloying and on the interaction with the support, leading to important changes in the final adsorption energy. The full list of GCN values per each class of adsorption sites is reported in Table SI 2 in the Supporting Information.

A scatter diagram of the adsorption energy versus generalized coordination number is sketched in Figure 4. First, we can

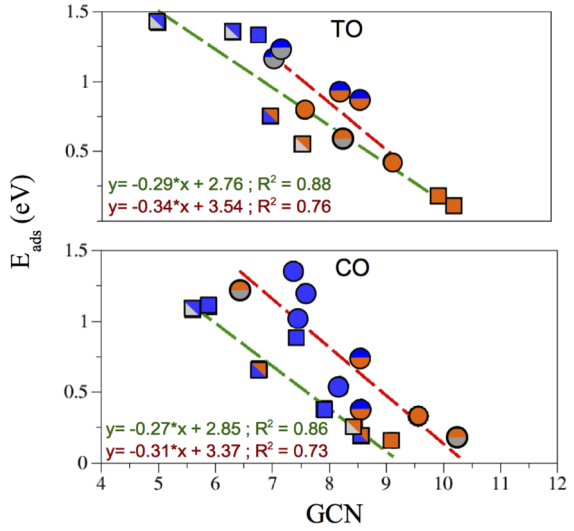

Figure 4. Adsorption energy, E_{ads} (eV) vs GCN for all different sites on TO_{82} (top panel) and CO_{86} (bottom panel), and for sandwich (circles, ○) and Ni@I (squares, □) chemical ordering. Circle and square symbols are colored according to Figure 2. The red (green) dashed line refers to the linear fit for sandwich (Ni@I) data.

generalize what has been observed for free and pure Pt nanoparticles.[25] Indeed, less-generalized coordinated sites bind a molecule stronger, even on alloyed and supported clusters. We note that an adsorption energy of <0.75 eV is ensured on sandwich structures for sites with a GCN > 8 and the same condition is satisfied when GCN ≥ 7 if we consider a Ni@I chemical ordering. Looking at the linear fitting of the calculated adsorption energies (indicated by the dashed lines in Figure 4), it is evident that (i) the interaction with molecular oxygen is weaker on CO than TO, and (ii) it is further reduced for Ni@I chemical ordering. The intercept seems to be dependent mostly on the chemical composition at the interface instead of the morphology.

The adsorption energy trends seen in Figures 3 and 4 can be partially rationalized in terms of the *d*-band center calculated

DOI: 10.1021/acscatal.6b00259
ACS Catal. 2016, 6, 4388−4393

for the supported PtNi systems (see Table SI 5 in the Supporting Information). A comparison between Ni and Pt monometallic *d*-centers confirms that pure Ni clusters bind O_2 much stronger than pure Pt, and there is evidence of a weakening of the adsorption of an oxygen molecule onto Ni@I, compared to the sandwich chemical ordering. Nonetheless, the GCN captures the small atomic distortions, caused by alloying and chemical ordering, better. Therefore, it seems to be a more robust descriptor to distinguish the huge variety of adsorption sites of a nanoparticle, and finally for its rational design as a nanocatalyst.

Taking into account the GCN values calculated for the gas phase monometallic nanoparticles,[25] we can claim that the oxide support and Ni alloying shift the GCN from a 2−7 window toward a 5−11 window, with a net decrease in the O_2 adsorption energy from a range of 0.5−2.2 eV to a range of 0.1−1.5 eV. Considering then our results and the activity-coordination plot in ref 26, although a direct comparison is not straightforward, PtNi nanoparticles with a diameter of at least 1.5 nm and an engineered chemical interface seem to be very promising nanocatalysts to improve the sluggish ORR reaction. In order to gain some insights on the predominant mechanism of the ORR on our supported PtNi systems, we calculated the adsorption map for a OOH molecule upon a limited number of sites. Adsorption energies and GCN values for the OOH adsorption are reported in Table SI 6 in the Supporting Information. We can summarize our findings as follows:

(i) The OOH is not stable on sites characterized by a low GCN and spontaneously dissociates to form an O atom and a OH group; and
(ii) The OOH is stable on high GCN sites, with an adsorption energy, with respect to the gas-phase molecular oxygen and hydrogen, of 3.5−3.8 eV.

We further estimate a difference in the activation barrier for the dissociation of molecular oxygen of ∼0.4 eV between high and low GCN sites. Although a full kinetic study is still needed, there is an indication that the associative/dissociative mechanisms are linked to high/low generalized coordination sites, respectively.

CONCLUSIONS

Although it is often claimed that the nanominiaturization of Pt catalysts is a practical way to reduce costs, as well as improve performance, the *a priori* identification of a route is not so obvious, because of many different effects. Here, we showed how the substrate and alloying effects influence the adsorption properties of $Pt_{shell}Ni_{core}$ nanoparticles supported on a rigid oxide, such as MgO(100). Indeed, we found that, already, at sizes as small as 1.5 nm, $Pt_{shell}Ni_{core}$ structures present a variety of nonequivalent sites and the O_2 adsorption varies widely from one site to another, respecting the general rule "lower site coordination = stronger interaction". We showed that, overall, the site coordination can be tuned by changing the chemical composition at the interface with the support. This relationship has been quantified by means of the generalized coordination number (GCN), which can distinguish symmetry-equivalent sites and establish a link between geometry, adsorption, and activity.[26] Our results can be summarized as follows:

(i) The support and the alloying shifts the GCN adsorption window (5−11) at a higher values, with respect to the gas phase (2−7);[25]
(ii) Hence, there are several sites characterized by a promising adsorption energy;
(iii) Molecular oxygen has a tendency to interact less on a cuboctahedral geometry than on an octahedral geometry;
(iv) Ni atoms in contact with the oxide support reduce the adsorption energy of molecular oxygen;
(v) there is an indication that the OOH formation occurs only on high GCN sites; and
(vi) there is an indication that the activation barrier for O_2 dissociation is strongly dependent on the GCN.

The choice of a Pt dopant with a large mismatch (e.g., Cu, Ni, Fe) works in the direction of increasing the generalized coordination of adsorption sites. The interaction strength window can be tuned by the design of the nanoparticle and by the chemical composition at the interface (which causes small rearrangements and then a different coordination of the adsorption sites). We hope that our observations based essentially on geometrical properties of supported bimetallic nanoparticles will open new routes to the rational design of multipurpose nanocatalysts.

ASSOCIATED CONTENT

Supporting Information

The Supporting Information is available free of charge on the ACS Publications website at DOI: 10.1021/acscatal.6b00259.

A more-detailed discussion on the (i) magnetism and stability of the considered PtNi nanoparticles; (ii) comparison between generalized coordination number and d-band center; and (iii) OOH adsorption and O_2 dissociation (PDF)

AUTHOR INFORMATION

Corresponding Authors

*E-mail: gian_giacomo.asara@kcl.ac.uk.
*E-mail: francesca.baletto@kcl.ac.uk.

Notes

The authors declare no competing financial interest.

ACKNOWLEDGMENTS

The authors thank the "Towards an Understanding of Catalysis on Nanoalloys" (TOUCAN) EPSRC Critical Mass Grant (No. EP/J010812/1) and Archer Supercomputing Service. L.O.P.B. acknowledges PAPIIT-UNAM (Project IA 102716). F.B. thanks further the financial support by the Royal Society grant (No. RG 120207). The authors would like to thank Alessandro De Vita for the useful discussion.

REFERENCES

(1) Schlögl, R. *Angew. Chem., Int. Ed.* **2015**, *54*, 3465−3520.
(2) Vines, F.; Gomes, J. R. B.; Illas, F. *Chem. Soc. Rev.* **2014**, *43*, 4922−4939.
(3) Cheng, D.; Yuan, S.; Ferrando, R. *J. Phys.: Condens. Matter* **2013**, *25*, 355008−355015.
(4) Tritsaris, G. A.; Greeley, J.; Rossmeisl, J.; Nørskov, J. K. *Catal. Lett.* **2011**, *141*, 909−913.
(5) Xin, H.; Holewinski, A.; Linic, S. *ACS Catal.* **2012**, *2*, 12−16.
(6) Li, D.; Wang, C.; Strmcnik, D. S.; Tripkovic, D. V.; Sun, X.; Kang, Y.; Chi, M.; Snyder, J. D.; van der Vliet, D.; Tsai, Y.; Stamenkovic, V. R.; Sun, S.; Markovic, N. M. *Energy Environ. Sci.* **2014**, *7*, 4061−4069.
(7) Zhang, X.; Lu, G. *J. Phys. Chem. Lett.* **2014**, *5*, 292−297.
(8) Wanjala, B. N.; Luo, J.; Loukrakpam, R.; Fang, B.; Mott, D.; Njoki, P. N.; Engelhard, M.; Naslund, H. R.; Wu, J. K.; Wang, L.; Malis, O.; Zhong, C.-J. *Chem. Mater.* **2010**, *22*, 4282−4294.

DOI: 10.1021/acscatal.6b00259
ACS Catal. 2016, 6, 4388−4393

(9) Strasser, P.; Koh, S.; Anniyev, T.; Greeley, J.; More, K.; Yu, C.; Liu, Z.; Kaya, S.; Nordlund, D.; Ogasawara, H.; Toney, M. F.; Nilsson, A. *Nat. Chem.* **2010**, *2*, 454−460.
(10) Stamenkovic, V. R.; Fowler, B.; Mun, B. S.; Wang, G.; Ross, P. N.; Lucas, C. a.; Marković, N. M. *Science (Washington, DC, U.S.)* **2007**, *315*, 493−497.
(11) Li, W.; Haldar, P. *Electrochem. Solid-State Lett.* **2010**, *13*, B47−B49.
(12) Cui, C.; Gan, L.; Li, H. H.; Yu, S. H.; Heggen, M.; Strasser, P. *Nano Lett.* **2012**, *12*, 5885−5889.
(13) Cui, C.; Gan, L.; Heggen, M.; Rudi, S.; Strasser, P. *Nat. Mater.* **2013**, *12*, 765−771.
(14) Mu, R.; Fu, Q.; Xu, H.; Zhang, H.; Huang, Y.; Jiang, Z.; Zhang, S.; Tan, D.; Bao, X. *J. Am. Chem. Soc.* **2011**, *133*, 1978−1986.
(15) Ahmad, R.; Singh, A. K. *ACS Catal.* **2015**, *5*, 1826−1832.
(16) Strasser, P. *Science* **2015**, *349*, 379−380.
(17) Fortunelli, A.; Goddard, W. A., III; Sementa, L.; Barcaro, G.; Negreiros, F. R.; Jaramillo-Botero, A. *Chem. Sci.* **2015**, *6*, 3915−3925.
(18) Norskov, J. K.; Abild-Pedersen, F.; Studt, F.; Bligaard, T. *Proc. Natl. Acad. Sci. U. S. A.* **2011**, *108*, 937−943.
(19) Medford, A. J.; Vojvodic, A.; Hummelshøj, J. S.; Voss, J.; Abild-Pedersen, F.; Studt, F.; Bligaard, T.; Nilsson, A.; Nørskov, J. K. *J. Catal.* **2015**, *328*, 36−42.
(20) Stamenkovic, V.; Mun, B. S.; Mayrhofer, K. J. J.; Ross, P. N.; Markovic, N. M.; Rossmeisl, J.; Greeley, J.; Nørskov, J. K. *Angew. Chem., Int. Ed.* **2006**, *45*, 2897−2901.
(21) Duan, Z.; Wang, G. *J. Phys. Chem. C* **2013**, *117*, 6284−6292.
(22) di Paola, C.; Baletto, F. *Phys. Chem. Chem. Phys.* **2011**, *13*, 7701−7707.
(23) Paz-Borbon, L. O.; Baletto, F. 2016, *arXiv:1604.02731*.
(24) Calle-Vallejo, F.; Loffreda, D.; Koper, M. T. M.; Sautet, P. *Nat. Chem.* **2015**, *7*, 403−410.
(25) Calle-Vallejo, F.; Martínez, J. I.; García-Lastra, J. M.; Sautet, P.; Loffreda, D. *Angew. Chem., Int. Ed.* **2014**, *53*, 8316−8319.
(26) Calle-Vallejo, F.; Tymoczko, J.; Colic, V.; Vu, Q. H.; Pohl, M. D.; Morgenstern, K.; Loffreda, D.; Sautet, P.; Schuhmann, W.; Bandarenka, A. S. *Science* **2015**, *350*, 185−189.
(27) Kresse, G.; Furthmüller, J. *Phys. Rev. B: Condens. Matter Mater. Phys.* **1996**, *54*, 11169−11186.
(28) Callejas-Tovar, R.; Diaz, C. A.; De La Hoz, J. M. M.; Balbuena, P. B. *Electrochim. Acta* **2013**, *101*, 326−333.
(29) Beermann, V.; Gocyla, M.; Willinger, E.; Rudi, S.; Heggen, M.; Dunin-Borkowski, R. E.; Willinger, M.-G.; Strasser, P. *Nano Lett.* **2016**, *16*, 1719−1725.
(30) Gan, L.; Heggen, M.; Cui, C.; Strasser, P. *ACS Catal.* **2016**, *6*, 692−695.
(31) Smerieri, M.; Pal, J.; Savio, L.; Vattuone, L.; Ferrando, R.; Tosoni, S.; Giordano, L.; Pacchioni, G.; Rocca, M. *J. Phys. Chem. Lett.* **2015**, *6*, 3104−3109.
(32) Schauermann, S.; Nilius, N.; Shaikhutdinov, S.; Freund, H. J. *Acc. Chem. Res.* **2013**, *46*, 1673−1681.
(33) Perdew, J. P.; Burke, K.; Ernzerhof, M. *Phys. Rev. Lett.* **1996**, *77*, 3865−3868.
(34) Kresse, G.; Joubert, D. *Phys. Rev. B: Condens. Matter Mater. Phys.* **1999**, *59*, 1758−1775.
(35) García, M. A.; Ruiz-González, M. L.; De La Fuente, G. F.; Crespo, P.; González, J. M.; Llopis, J.; González-Calbet, J. M.; Vallet-Regí, M.; Hernando, A. *Chem. Mater.* **2007**, *19*, 889−893.
(36) Di Paola, C.; D'Agosta, R.; Baletto, F. *Nano Lett.* **2016**, *16* (4), 2885−2889.
(37) Wang, C.; Chi, M.; Li, D.; Strmcnik, D.; van der Vliet, D.; Wang, G.; Komanicky, V.; Chang, K.-C.; Paulikas, A.; Tripkovic, D.; Pearson, J.; More, K.; Markovic, N. M.; Stamenkovic, V. R. *J. Am. Chem. Soc.* **2011**, *133*, 14396.
(38) Calvo, F.; Fortunelli, A.; Negreiros, F. R.; Wales, D. J. *J. Chem. Phys.* **2013**, *139*, 111102−111104.
(39) Bray, J. M.; Schneider, W. F. *Langmuir* **2011**, *27*, 8177−8186.
(40) Eichler, A.; Mittendorfer, F.; Hafner, J. *Phys. Rev. B: Condens. Matter Mater. Phys.* **2000**, *62*, 4744−4755.

DOI: 10.1021/acscatal.6b00259
ACS Catal. 2016, 6, 4388−4393